IEEE Transactions on Nuclear Science, Vol. NS-33, No. 6, December 1986

ANALYSIS OF THE ION SPOT PHENOMENON ON BEAM-CHARGED DIELECTRICS*

Gordon McKeil and K.G. Balmain
Department of Electrical Engineering
University of Toronto
Toronto, Canada M5S 1A4

Abstract

Computer simulation of particle trajectories in two dimensions using a simple static accumulated charge model reveals the mechanism for the focussing of ions into a central, sharply defined "spot", duplicating the luminescent spot which did not arc-discharge observed during laboratory exposure of polymer film to monoenergetic electrons and low energy ions. A model which follows the time evolution of such charging situations is developed and initial results are presented.

Introduction

Spacecraft insulating materials charged by electrons while in orbit are simultaneously exposed to protons and other positive particles. The flux of these positive particles has been measured in geosynchronous orbit to be typically about 10% of the electron flux [1]. Thus some neutralization of the negative electron surface charge which accumulates on the exposed insulating materials of a spacecraft can be expected. Previous laboratory experiments [2] together with theoretical results reported in this paper show that, due to strong focussing of the incoming positive particles, the degree of neutralization is not uniform over the entire exposed area, but can be confined to a small region of roughly complete neutralization with the remaining surface affected only slightly.

In laboratory experiments [1,2], to investigate the effects of positive ions during charging, sheets of polymer were exposed to combined beams of monoenergetic electrons and low energy ions. The sheets were laid over a metal substrate and covered by a metal plate with a circular aperture. With electrons alone luminescence due to electron impact was initially seen over the entire exposed polymer, and the luminescence faded as irradiation continued. When ions were included, a bright central luminescent spot which did not fade was observed.

The spot faded when the ion source was turned off, quickly reappeared when the source was restored, and expanded when the ion current was increased. This "ion spot" was interpreted as a region of ion neutralization of the embedded electron charge, which permits the electrons to strike the polymer with most or all of the beam energy to produce strong luminescence. For a 1 cm² aperture the boundaries of the spot were ill defined, while, with the 15.9 cm² aperture, the boundaries were exceptionally sharp. Subsequent arc discharges avoided the spot area. Other investigators [3] have reported situations displaying some similar luminescence characteristics, involving a surface with a high negative bias in a plasma.

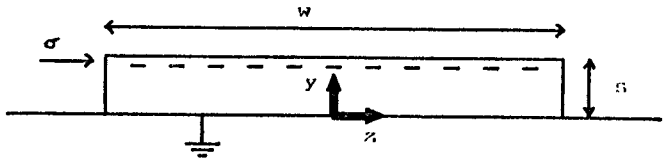

Fig. 1
Charge distribution used to represent the charge on a polymer sheet after irradiation by an electron beam. The parameters are the surface charge density σ, strip width w, and sheet thickness s. Coordinate axes , y, z, used in this paper are also shown.

This paper describes theoretical calculations which have successfully reproduced the ion spot phenomenon in two dimensions. Computer simulations have been undertaken using two different models for the charge accumulation on polymer surfaces, referred to as the simple static model and the time evolution model.

Simple Static Model

Here the flux at the surface is calculated for an ion beam incident upon a polymer sheet previously charged by an electron beam. A simple two-dimensional charge distribution was used to represent the total free and bound surface charge on the polymer sheet after electron irradiation. The charge distribution, shown in Figure 1, consisted of a strip of negative surface charge of uniform density, infinite in length, but of finite width, held in free space over a ground plane. For field calculations, the ground plane is replaced by image charges. The parameters for the calculations were the surface charge density σ, strip width w, and sheet thickness (the charge to ground plane separation) s. Figure 1 also shows the coordinate system used throughout this paper. The direction across the strip width is denoted as z and the direction perpendicular to the strip surface is denoted as y.

Trajectories were calculated, using a third order Runge-Kutta method [4], for low energy ions directed towards this charge distribution and released at different positions across the width of the strip. The image forces of the incident ion in the ground plane were included quasi-statically but were relatively insignificant. A typical set of ion trajectories is shown in Figure 2. These trajectories show that some particles rebound completely from the dipole-like field.

The ion beam flux at the specimen surface was then inferred from the calculated trajectories. Let us define ζ to be the z - coordinate at which an ion trajectory initially began, far from the surface, and use z as the coordinate for the ion trajectory when it reaches the surface level. If two neighboring trajectories initially began at ζ_i, ζ_{i+1} and reached the surface at z_i, z_{i+1}, then the average incident flux at the surface for z between z_i and z_{i+1} is

$$f(z) = f_0 \left| \frac{\zeta_{i+1} - \zeta_i}{z_{i-1} - z_i} \right| \qquad (1)$$

where f_0 = ion beam flux far from the specimen.

If trajectories cross and more than one pair of

*Work supported by the U.S. Air Force Weapons Laboratory, by AFOSR Grant 84-0342 and by the Natural Sciences and Engineering Research Council of Canada through Grant A-4140.

0018-9499/86/1200-1396$01.00 © 1986 IEEE

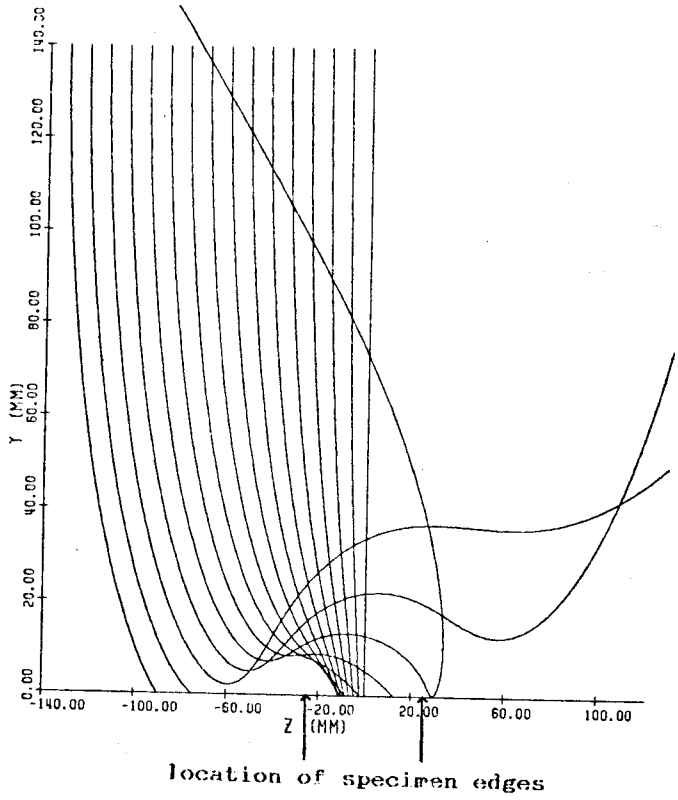

Fig. 2 A typical set of ion trajectories.

neighboring trajectories bracket a point, z, on the surface, then the flux contributions of each pair must be summed.

$$f(z) = f_o \sum_{\{i \mid z \in [z_i, z_{i+1}]\}} \left| \frac{\zeta_{i+1} - \zeta_i}{z_{i+1} - z_i} \right|$$

$$f_o \sum_i H(z, [z_i, z_{i+1}]) \left| \frac{\zeta_{i+1} - \zeta_i}{z_{i+1} - z_i} \right| \qquad (2)$$

where H is a kind of step function. For point z, and set A,

$$H(z, A) = \left\{ \begin{array}{l} 1 \ , \ \text{if } z \in A \\ 0 \ , \ \text{if } z \notin A \end{array} \right\}$$

Using equation 2, the ratio of incident ion flux at the specimen surface to the flux far from the surface, $f(z)/f_o$, was calculated. This is not the same as the net charge deposited onto the surface as secondary electron emission has not been accounted for. The results are presented in Figure 3 for 10eV protons incident upon strips with a surface charge density of -70 nC/cm², a sheet thickness of 50 μm, and strip widths of 5, 15, 25, and 50 mm. The surface potential near the centre of the strip was in all cases -4 kV.

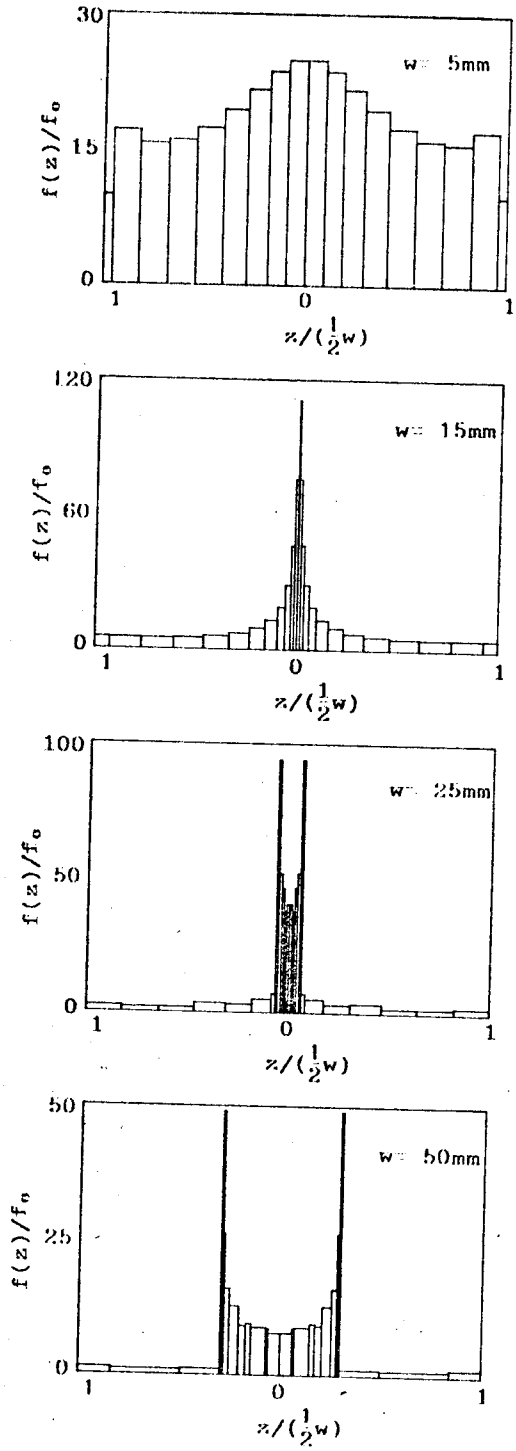

Fig. 3
Ratios for various specimen widths w, of ion flux at surface to flux far away, $f(z)/f_o$, as a function of position across sepcimen, normalized by the half width, $z/(\frac{1}{2}w)$

The relative ion flux is plotted in Figure 3 as a function of the position across the specimen, normalized with respect to the half-width ($z/(\frac{1}{2}w)$). The central regions of high ion flux appear to be the 2-dimensional analogues of the ion spots observed in the laboratory. As in the laboratory, the ion spot boundaries are ill defined for the small specimen widths, but are very sharp for larger specimens.

The spot forms over a wide range of conditions. For the case of the 50 mm wide strip, the spot forms over a range of at least -5 to -1000 nC/cm² (.3 to -56 kV). Similar results were obtained for sheet thickness of 25 and 100 μm. We are dealing with an electrostatic situation and therefore the trajectories are independent of the ion mass, provided the initial energy is unchanged. The results presented are correct for any particles with the charge of a proton. Further, a change in the surface charge or the ionic charge magnitude produces the same trajectories as an inversely proportional change in the initial energy. Thus, from the results obtained by varying the surface charge, it can be inferred that spot formation occurs for a surface charge of -70 nC/cm² over a range of initial energies of at least 0.7 to 700 eV. However, although the trajectories are independent of ion mass and combined changes of charge and initial energy, the speeds at which these trajectories are traversed are not equal. Thus, while the incident ion fluxes are the same, the penetration depths and secondary electron emission properties will vary, resulting in different net charge deposition rates.

Mechanism for Spot Formation

Closer examination of the trajectories and equations 1 and 2 reveals the mechanism for spot formation. If, in equation 1, we allow the two neighboring trajectories to approach one other, we obtain

$$f(z) = f_o \lim_{\substack{z_i \to z \\ z_{i+1} \to z}} \left| \frac{\zeta_{i+1} - \zeta_i}{z_{i+1} - z_i} \right|$$

$$= f_o \left| \frac{d\zeta(z)}{dz} \right| \qquad (3)$$

Here we have generalized $\zeta(z)$ to be a function of z, so that $\zeta(z)$ is the initial position measured across the specimen width (measured when far from the surface) for the trajectory which finally reaches the surface level at position z. If the ion trajectories cross, then $\zeta(z)$ will be a multi-valued relation (more than one ion may hit the same position on the surface). In such cases, ζ should be divided into several single-valued functions, ζ_k, each valid over its own domain, D_k. In a manner analogous to equation 2, when calculating the surface ion flux, the contribution of each relevant section, ζ_k, must be included.

$$f(z) = f_o \sum_k H(z, D_k) \left| \frac{d\zeta_k(z)}{dz} \right| \qquad (4)$$

To clarify the application of equation 4, Figure 4 shows, for the 50 mm width case of Figure 3, the relation $\zeta(z)$ and compares it to the relative surface ion flux, $f(z)/f_o$. Both the surface ion flux and the relation $\zeta(z)$ plotted were calculated from the same set of trajectory results, (z_i, ζ_i) - the flux via equation 2 and $\zeta(z)$ via cubic spline interpolation. In Figure 4 is shown the division, for that example, of $\zeta(z)$ into three single-valued functions $\zeta_k(z)$, and their domains

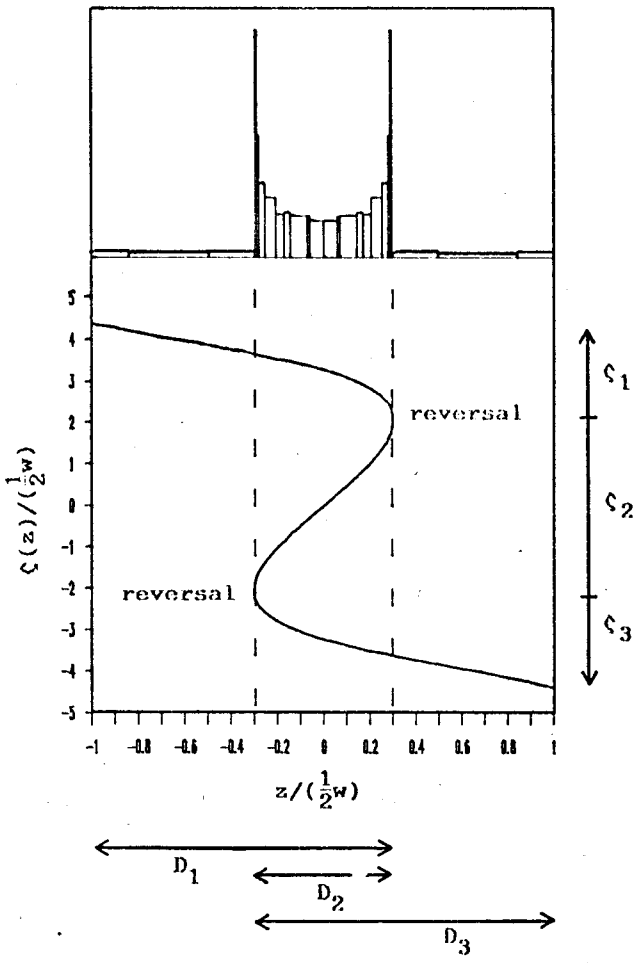

Fig. 4 Comparision of initial vs. final ion position curve $\zeta(z)$, with resulting surface ion flux pattern $f(z)/f_o$, for the w= 50mm case from figure 3

D_k. The reversals indicated are a consequence of crossing ion trajectories. The surface flux is porportional to the projection of the absolute values of the slopes of the trajectory curves $\zeta_k(z)$, as drawn, down onto the z-axis. The region of steep slopes, reflecting high ion concentrations, for z between the reversal points corresponds to the ion spot. The smooth behaviour of the relation $\zeta(z)$, reflects a natural continuity in the variation of the trajectories with initial position. Upon projection onto the z-axis, however, the reversals provide for very steep slopes immediately inside the spot region and shallow slopes immediately outside. Thus the smoothly varying ion trajectories can produce the ion spot with its discontinuously sharp boundaries.

Time Evolution Model

Model Development

The static model successfully duplicates the ion spot and has the appeal of simplicity. However it deals only with ions incident upon pre-charged surfaces and does not allow for time development of the surface charge. It cannot duplicate the laboratory observation that the spot size increases with the ion beam current. The high concentrations in the ion spot can be expected to strongly affect the surface charge distribution and

the trajectories of subsequently incident ions and electrons. A model which follows such evolving features of accumulating surface charge is required.

The time evolution model developed here solves for the surface charge distribution as a function of time, on a polymer sheet exposed simultaneously to monoenergetic electron and ion beams. As in the static model, the two-dimensional specimen geometry of an infinite strip of polymer over a grounded substrate plane is used. This model builds on previous work [5] but all development presented here is new.

The net surface charge accumulated is affected by the incident particle flux, the secondary electron emission due to particle impact and the internal conductivity. Conductivity effects were not included in the model. The model restricts itself to low and moderate electron and ion energies resulting in penetration depths small compared to the sheet thickness and to materials with low inherent bulk conductivity. Thus charge transport from the surface through to the grounded substrate due to inherent conductivity or radiation induced conductivity need not be considered further. Due to the small penetration depths, the charge can be considered to be all at the surface and any radiation induced conductivity between near-surface charge layers will not affect the total surface charge. Lateral radiation induced conductivity may occur, particularly at the spot boundaries where fields should be high, but this was neglected in the model. However, the laboratory observations indicate that lateral conduction is not of overriding importance, for the sharp ion spot boundaries could be expected to be blurred if lateral conduction dominated. To introduce secondary electron emission into the analysis, define the coefficient C to be the average total charge deposited on the surface per incident particle. Thus for a proton which upon impact is itself embedded and, on average, causes the ejection of 1.2 electrons, we would have C = +2.2 proton charge.

The following expressions were used to describe the electron emission of polymers bombarded by electron [6]. With E designating the energy in keV of the incident particle, and θ being the angle of incidence from the target surface normal, we have,

describing secondary electron emission

$$SE = K\, E^{-0.725} \exp(2(1-\cos\theta))$$

where K = 1.55 for Teflon
= 0.68 for Kapton

describing electron backscattering

$$BS = (0.1E^{-0.2})\cos\theta$$

and the coefficient C, is given by

$$C = 1 - SE - BS$$

The electron emission of polymers bombarded by ions is not well reported. For other materials, the emission due to ion bombardment is generally greater than for electron bombardment for this energy range (SE ~ 1 for metals and semiconductors, SE ~ 10 for non-organic dielectrics) [7]. For this model, a simple, conservative approximation was used. For ions, with E and θ defined as before, we have

$$SE \sim .4\, E^{\frac{1}{2}}$$

$$C = 1 + SE \quad .$$

The coefficient C is treated as a function of time because the surface charge distribution changes with time. With crossing trajectories, particles may strike the same point on the specimen with different angles and thus have different coefficient C. Therefore C is also treated as a function not of the final position at which it reaches the surface, but of the initial trajectory position, $C = C(\zeta, t)$. Adding this coefficient to equation 4, we may express the rate of surface charge deposition $\frac{d\sigma}{dt}$, across the specimen width as below.

$$\frac{d\sigma(z,t)}{dt} = f_o \sum_k H(z, D_k) \left| \frac{d\zeta_k}{dt}(z,t) \right| C(\zeta_k(z,t), t) \qquad (5)$$

Here ζ_k has been extended to be a function of time. The domains D_k, will also change with time, as may the possible values of k, as new single-valued sections become required and old ones merge together.

At some points, such as the reversal points of Figure 4, the derivative $\frac{d\zeta_k}{dt}$, goes to finity and $\frac{d\sigma}{dt}$ will have a pole. The infinities may be avoided by considering the charge accumulated over a finite section of the specimen instead of the charge density. For this two-dimensional model, this means making a division across the specimen width, $\{z_1, z_2, z_3, \ldots, z_N\}$, and considering the linear charge density ρ_n, on each small sub-strip section.

$$\rho_n(t) = \int_{z_n}^{z_{n+1}} \sigma(z,t)\, dz \qquad (6)$$

Substituting into equation 6 from equation 5, we obtain,

$$\frac{d\rho_n}{dt}(t) = f_o \sum_k \int_{z_n}^{z_{n+1}} H(z, D_k) C(\zeta_k(z,t), t) \left| \frac{d\zeta_k}{dt}(z,t) \right| dz \qquad \ldots(7)$$

The model is physically tenable as the value of $\frac{d\rho_n}{dt}$ remains finite regardless of the division used. The fineness of the division is limited mainly by the computational accuracy of the trajectory calculations.

Since an electron initially released at a particular position ζ is constrained to go to only one point on the specimen, the functions ζ_k, will be one-to-one, or, equivalently, monotonic. Therefore, the derivatives $\frac{d\zeta_k}{dz}$, will each be either always positive or always negative over their entire domain D_k, and we can define α_k to be the sign of $\frac{d\zeta_k}{dt}$ with α_k independent of z. We can proceed,

$$\frac{d\rho_n}{dt}(t) = f_o \sum_k \int_{z_n}^{z_{n+1}} H(z, D_k) C(\zeta_k(z,t), t) \alpha_k \frac{d\zeta_k}{dt}(z,t)\, dz$$

$$= f_o \sum_k \alpha_k \int_{\zeta(z_n,t)}^{\zeta(z_{n+1},t)} C(\zeta_k(z,t), t)\, d\zeta \qquad (8)$$

where, to simplify notation, ζ_k is extended as a constant function outside of D_k. That is, if $D_k = [a, b]$, then ζ_k is extended as,

$$\zeta_k(z,t) = \begin{cases} \zeta_k(a,t) & , \text{ if } z \le a \\ \zeta_k(z,t) & , \text{ if } z \in D_k \\ \zeta_k(b,t) & , \text{ if } z \ge b \end{cases}$$

If $C(\zeta,t)$ may be approximated by a constant over each interval, then equation 8 simplifies to,

$$\frac{d\rho_n(t)}{dt} = f_o \sum_k |\zeta_k(z_{n+1},t) - \zeta(z_n,t)| C_{nk}(t) \qquad (9)$$

With equation 8 and enough calculated trajectories to adequately define ζ_k and C, the instantaneous surface charge deposition rate can be computed. However, although the deposition rates $\frac{d\rho_n}{dt}$ are finite, they remain strongly peaked for sub-strips near certain positions such as the reversals of Figure 4. Further, these deposition rate peaks move across the specimen with time. This makes attempts to follow the time evolution of surface charge problematic. The depositon rate can be approximated as constant in time for less than the short period that is required for the peaks to move across the specimen a distance equal to the narrow peak width. The computation time would be too great to make the full trajectory calculations required to use equation 8 at such short time intervals for the whole charging process.

The underlying relations $\zeta(z,t)$, $C(\zeta,t)$, are more smoothly varying, however. Thus calculations of these curves could be made at less frequent intervals and an interpolation method used. The domains D_k, vary in time and because of this it is less complex when comparing curves for different times to take the inverse of the relation $\zeta(z,t)$ and consider $z(\zeta,t)$. That is, to consider the final ion position z at the specimen surface as a function of the initial position ζ. It was found that for small time changes the variation in $z(\zeta,t)$ could be approximated with a combination of linear amplitude and scale factors. For small intervals Δt about a particular time t, constants A,B, could be found to satisfy,

$$z(\zeta, t+\Delta t) \doteq (1+A\times\Delta t) \times z((1+B\times\Delta t)\times\zeta, t) \qquad (10)$$

This suggested the following interpolation procedure. If the curves z, C, have been calculated for times t_1, t_2, then the curves for other times can be estimated as by,

$$z(\zeta,t) = z((1+B\times(t-t_1))\times\zeta, t_1) \times \left(\frac{t-t_2}{t_1-t_2}\right) + z((1+B\times(t-t_2))\times\zeta, t_2) \times \left(\frac{t-t_1}{t_2-t_1}\right) \qquad (11)$$

$$C(\zeta,t) = C((1+B\times(t-t_1))\times\zeta, t_1) \times \left(\frac{t-t_2}{t_1-t_2}\right) + C((1+B\times(t-t_2))\times\zeta, t_2) \times \left(\frac{t-t_1}{t_2-t_1}\right) \qquad (12)$$

where B is choosen as follows. The trajectory at time t_1 which hits the extreme right-most edge of the specimen ($z = +\frac{1}{2}\omega$) should be scaled to the trajectory at t_2 which also hits the right-most edge. This means that if ζ_{1+} and ζ_{2+} are the initial positions for the trajectories which hit the right-most edge, that is

$$z(\zeta_{1+}, t) = +\tfrac{1}{2} w$$

$$z(\zeta_{2+}, t) = +\tfrac{1}{2} w$$

then B should satisfy

$$\zeta_{2+} = (1+B\times(t_2-t_1))\times\zeta_{1+}$$

Analogously, for the left-most specimen edge, if ζ_{1-} and ζ_{2-} are the initial positions such that

$$z(\zeta_{1-}, t) = -\tfrac{1}{2} w$$

$$z(\zeta_{2-}, t) = -\tfrac{1}{2} w$$

then B should satisfy

$$\zeta_{2-} = (1+B\times(t_2-t_1))\times\zeta_{1-}$$

To best satisfy these two conditions, we choose

$$B = \frac{1}{(t_2-t_1)}\left(\left(\frac{\zeta_{2+}^2 + \zeta_{2-}^2}{\zeta_{1+}^2 + \zeta_{1-}^2}\right)^{1/2} - 1\right)$$

Different methods for choosing parameter B were considered. The method used was chosen as the most reliable at producing matches in the sense of equation 10.

The interpolated function $z(\zeta,t)$, from equation 11 may be inverted to yield $\zeta_k(z,t)$, and D_k. These, together with $C(\zeta,t)$ from equation 12 can be used in equation 8 to obtain the charge deposited $\Delta\rho_n$, during the time period t_1 to t_2.

$$\Delta\rho_n = \int_{t_1}^{t_2} \frac{d\rho_n}{dt}\, dt$$

$$= f_o \int_{t_1}^{t_2} dt \sum_k \alpha_k \int_{\zeta_k(z_n,t)}^{\zeta_k(z_{n+1},t)} d\zeta\, C(\zeta_k(z,t),t) \qquad (13)$$

Modeling Calculation Procedure

The geometry of the uncharged specimen is defined by the strip width, sheet thickness, and material dielectric constant and electron emission properties. The electron and ion beams are each defined by beam energy and initial flux and, in the ion case, the particle mass. A division of the specimen surface is made to define the sub-sections ρ_n, as in equation 6. Initially, at time t = 0, the trajectory curves $\zeta(0)$, C(0), may be easily calculated for both electrons and ions by assuming no deflection of incoming beams.

An initial step in time, to $t = t_1$, is chosen. The surface charge for t_1 is first estimated by assuming constant, undeflected electron and ion fluxes for the period t = 0 to t_1. Using this first surface charge estimate, the trajectory curves $\zeta_k(t_1)$, $C(t_1)$, are calculated. Then the curves for the period 0 to t_1 are interpolated using equations 11, 12 and a final calculation of the surface charge deposited for each sub-section $\Delta\rho_n$, for the period 0 to t_1 is made using equation 13. A measure of the error for this initial step can be obtained by comparing the final calculation of the deposited surface charge to the first estimate.

A second step in time, to t_2, is chosen. The trajectory curves $\zeta_k(t)$, C(t), for the period t_1 to t_2 are extrapolated from $\zeta_k(0)$, C(0), and $\zeta_k(t_1)$, $C(t_1)$ using equations 11 and 12. These extrapolated curves are used with equation 13 to estimate the electron and ion charge depositions $\Delta\rho_n$, for the period t_1 to t_2, and to arrive at a first estimate for the total surface charge at time t_2. Using this first estimate, the curves $\zeta_k(t_2)$, $C(t_2)$ are calculated for electrons and ions. The curves for the time period t_1 to t_2 are interpolated using $\zeta_k(t_1)$, $C(t_1)$, and $\zeta_k(t_2)$ and $C(t_2)$ with equations 11 and 12, and the final calculation of the electron and ion charge

depositions $\Delta\rho_n$, for the period t_1 to t_2 is made using equation 13, to arrive at a final calculation of the surface charge at time t_2. Again a measure of the error for this step can be obtained by comparing the final calculation to the first estimation of the deposited surface charge.

A third step, to t_3, and subsequent steps are chosen and the electron and ion charge depositions for each step are calculated in the manner described for the step t_1 to t_2. After repeated iterations, the surface charge should approach a steady state equilibrium.

Results

The developing surface charge for a teflon strip 50 mm wide and 100 μm thick exposed to a 20 keV electron beam with an intensity of 50 nC/cm² and a 100 eV lithium beam at 5nC/cm² is shown in Figure 5. Each of the three curves shows the total surface charge accumulated on the specimen from the beginning of irradiation to the time during early exposure indicated for that curve. The surface charge is due to the combined effects of the electron and ion beams. The distinctive ion spot pattern with the central region of more positive surface charge and peaked edges, can be seen emerging and concentrating with continued exposure. However, problems associated mainly with the increasing complexity of ion trajectories as the surface charge develops have so far prevented the computation from progressing to a steady state. The sharply peaked edges of the ion spot pattern shown in Figure 5 result in transverse electric fields at the spot boundary of up to 10^6 V/m. It is not expected that discharges will be initiated at the ion spot because higher fields, of about 5×10^6 V/m are found at the very edge of the sample strip and discharges observed experimentally have avoided the ion spot, rather than being initiated there.

Conclusions

The ion spot phenomenon has been successfully simulated theoretically in two dimensions by calculating trajectories over a very simple model for the accumulated surface charge on a polymer sheet pre-charged by electron irradiation. The mechanism for spot formation has been found and shown to possess scaling properties to indicate ion spot occurrence over a wide range of conditions. The problems of following the time evolution of the charge distribution resulting from the strongly concentrated and time-varying incident ion flux profiles have been investigated and largely overcome by use of interpolation of the underlying trajectory properties, which vary more continuously. Initial results of the time evolution model have shown the emergence of the ion spot pattern from the developing surface charge on a polymer sheet during simultaneous irradiation by electrons and ions.

The combination of successful duplication by a very simple model, scaling properties and occurrence over a wide range of conditions, and emergence from the evolving surface charge during simultaneous electron and ion irradiation, shows the phenomenon to possess a robust nature. This invokes an expectation that the ion spot will be present in situations involving different charged particle environments and different specimen geometries which prevail during both laboratory testing and actual space flight conditions.

References

[1] M. Gossland, and K.G. Balmain, "Incident ion effects on polymer surface discharges", IEEE Trans. Nucl. Sci., Vol. NS-30, no.6, pp.4302-4306, Dec. 1983.

[2] K.G. Balmain, A. Battagin, and G.R. Dubois, "Thickness scaling for arc discharges on electron-beam-charged dielectrics", IEEE Trans. Nucl. Sci., Vol. NS-32, no.6, Dec. 1985.

[3] J.E. McCoy, and Andrei Konradi, "Sheath effects on a 10 meter high voltage panel in simulated low earth orbit plasma", NASA Conf. Pub. 2071, AFGL-TR-79-0082, Spacecraft Charging Tech. - 1978, pp. 315-340.

[4] C. Weber, "Numerical solution of Laplace's and Poisson's equations and the calculation of electron trajectories and electron beams", in book, Focussing of Charged Particles, Vol.1, Edited by A. Septier, Academic Press, New York, pp.45-98.

[5] R.D. Reeves, and K.G. Balmain, "Two-dimensional electron beam charging model for polymer films", IEEE Trans. Nucl. Sci., Vol. NS-28, no.6, pp.4547-4552, Dec. 1981.

[6] J.A. Wall, E.A. Burke, and A.R. Frederickson, "Results of literature search on dielectric properties and electron interaction phenomena related to spacecraft charging", Peoc. of the Spacecraft Charging Technology Conference - 1977, NASA TMS-73537, pp.569-592.

[7] K.M. Krebs, "Recent advances in the field of ion-induced kinetic electron emissions from solids", Vacuum, Vol.33, no.9, pp.555-563, 1983.

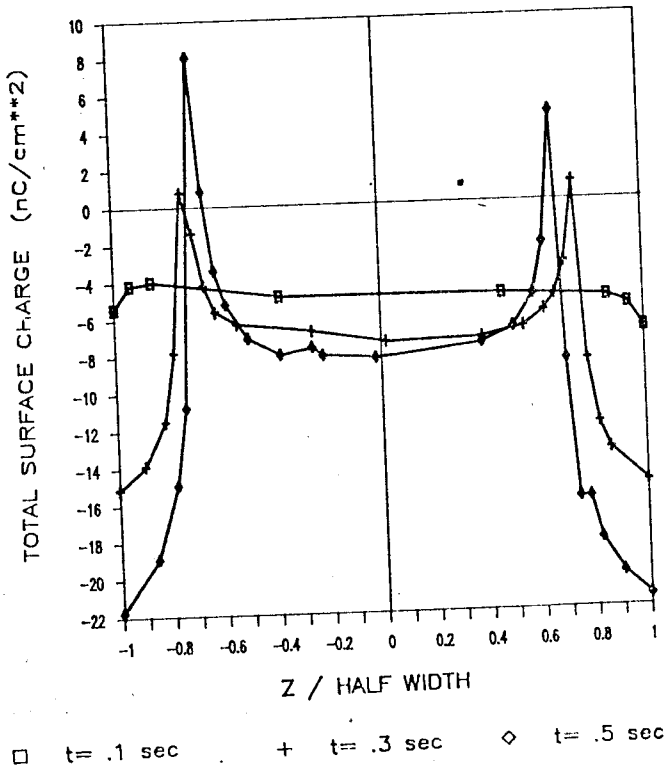

Fig. 5
Results for time evolution model showing the developing surface charge due to combined effect of electron and ion beams for three different times during early irradiation of a 50mm wide, 100μm thick, Teflon strip exposed to 20keV electrons at 50nC/cm^2 and 100eV lithium ions at 5nC/cm^2.